# Effective Thermal Conductivity of Lithium-Ion Battery Electrodes in Dependence on the Degree of Calendering

*Julia C. Gandert,\* Marcus Müller, Sabine Paarmann, Oliver Queisser, and Thomas Wetzel*

The thermal conductivity represents a key parameter for the consideration of temperature control and thermal inhomogeneities in batteries. A high-effective thermal conductivity will entail lower temperature gradients and thus a more homogeneous temperature distribution, which is considered beneficial for a longer lifetime of battery cells. Herein, the impact of the microstructure within the porous electrode coating obtained by different compression rates and its thermal contact to the current collector is investigated as both factors significantly determine the overall conduction through the electrode. The effective thermal conductivity of two graphite anodes and two lithium nickel manganese cobalt oxide cathodes is evaluated at different compression rates. It is found that the thermal conductivity does not have a monotone dependence on the porosity with changing compression rates. The results show a strong correlation with the adhesion strength, thus a significant impact of the thermal contact resistance between the coating and current collector is assumed.

## 1. Introduction

In the whole field of mobile applications and especially in the automotive sector, lithium-ion batteries have gained serious importance during the last two decades. Due to both, sustainability reasons and customer requirements, it is essential to keep the batteries small and lightweight and exchanges of batteries or even whole devices as low as possible. Thus, it is important to refine the cell configurations to enhance the battery performance and lifetime, which is so far mostly advanced with regard to the electrochemical behavior to increase the energy and power density.

The impact of the thermal behavior of battery cells is still often neglected, although it has a huge influence on the performance and aging of batteries.[1–5] Optimizing the thermal material properties can decelerate aging and improve the performance of batteries.[6]

To do so, the effects of design changes on the cell behavior have to be known, meaning that we need to understand the impact of different influencing factors, e.g., the microstructure of the electrodes and according defects, on the thermal behavior of the battery cells. This concerns both the absolute cell temperature and the temperature distribution within the cell. For this, the significant impact factors on the thermal behavior—density, specific heat capacity, and thermal conductivity—, which are highly impacted by the material composition and microstructure, need to be known. High values of the product of density and specific heat capacity imply a slow temperature response and thus only a slight increase of the temperature during peak loads. High thermal conductivities result in lower temperature gradients as a lower temperature difference along the cell is needed to conduct the same amount of heat out of the system.

As shown by several authors, the aging is excessively accelerated by large temperature gradients perpendicular to the electrodes.[1,7] Thus, a thermal conductivity as high as possible should be obtained and contact resistances between the layers should be minimized.

A lot of research was done on the determination of the thermal conductivity of the single components of battery cells from graphite anodes over separators to cathodes with different active materials.[8–12] A comprehensive overview was given by Steinhardt et al.[13]

Realistic values of density, specific heat capacity, and thermal conductivity are needed for the parameterization of thermal battery models, which are used to simulate the temperature distribution within battery cells. As the measurement of the temperature within the cells still poses a great challenge and the effects of inline measurement devices on the electrical cell behavior are not yet fully understood,[14,15] modeling is crucial to estimate the core temperature of the cells. However, those models are based on a lot of assumptions like the homogenization of the transport properties of the whole battery stack[16–18] and the neglection of contact resistances. Moreover, they are difficult to validate[15] and

J. C. Gandert, S. Paarmann, O. Queisser, T. Wetzel
Institute of Thermal Process Engineering (TVT)
Karlsruhe Institute of Technology (KIT)
Kaiserstraße 12, D-76131 Karlsruhe, Germany
E-mail: julia.gandert@kit.edu

M. Müller
Institute for Applied Materials – Energy Storage Systems (IAM-ESS)
Karlsruhe Institute of Technology (KIT)
Hermann-von-Helmholtz-Platz 1, D-76344 Eggenstein-Leopoldshafen, Germany

the calculated temperature field is only as accurate as the data provided for the thermal material properties.

Multiple authors have investigated the influence of the microstructure configured by different mixing,[19–21] coating and drying,[19,22,23] and calendering[19,24–29] conditions on the mechanical and electrical properties of the electrodes. It can be assumed that the transformation of the microstructure due to the different processes affects the thermal transport properties as well.

However, there is a significant research gap concerning the impact of microstructure changes and defects on thermal electrode behavior. This study aims to shed light on the changes in the most critical transport property when it comes to thermal gradients, the thermal conductivity, caused by alterations in the microstructure due to calendering. We used calendering for the configuration of the microstructure as it not only influences the porosity but also creates mechanical defects and has a huge impact on the interface between coating and current collector. The changes during the process and the most important variables and components are schematically depicted in **Figure 1**.

The goal of the calendering process is the enhancement of the electrochemical properties like electrical conductivity and energy density as well as the homogenization of the mechanical structure.[30] Hereby, the mechanical stability of the coating and interfaces is improved,[25] aging mechanisms during operation occur more homogeneously,[30] and the lifetime is increased due to the enhanced adhesion strength.[19] The compression of the coating reduces the porosity and alters the whole microstructure. Many authors have shown that calendering has a significant impact on mechanical and electrochemical material properties[26,27,31,32] and can entail different defect patterns. Too high compression rates result in particle breakage,[33,34] wrinkles and waves in the current collector and coating,[34,35] penetration of rigid particles into the current collector,[25,27,28,34,36–40] coiling up of the electrode[34] and resulting delamination of the coating, restrictions in lithium-ion diffusion,[31] a high tortuosity, and consequently wetting problems.[26,35,41] Low compression rates can lead to poor electrical conductivity[31] and low adhesion strength.[28,29]

There is only one study known to the authors investigating the dependence of the thermal conductivity of the coating material on the applied compression pressure before the measurement,[42] suggesting an improvement of the thermal conductivity with increased pressure. As those investigations were made without a current collector they leave out the impact of the interface. Moreover, Richter et al.[11] showed the impact of varied pressures

during the measurement, also leading to higher thermal conductivities with higher applied pressure.

There are few models known that describe the thermal conductivity with respect to the porosity.[43,44] However, no experimental studies investigating this interdependency are known, thus changes in the compression rate were not taken into account here, which impairs the comparability to the results obtained in this study.

In this work, two cathodes with NMC622 and NMC811 as active materials and two graphite anodes with different starting thicknesses after the coating and drying processes were examined. Hereby, the density $\rho$, specific heat capacity $c_p$, and thermal diffusivity $\kappa$ of the coated electrodes were measured to determine the thermal conductivity $\lambda$ according to Equation (1).

$$\lambda = \kappa \cdot \rho \cdot c_p \tag{1}$$

The latter was evaluated for varyingly strong calendered sheets and its dependency on the compression rate was determined. Furthermore, this study compares the experimentally determined data to modeling approaches, points out the limits for their use, and gives recommendations for their improvements.

## 2. Results and Discussion

This section discusses the experimental results concerning the effective thermal conductivity. Moreover, the uncertainty of thickness measurements is analyzed and a comparison of the data with existing models is presented. For details of the sample preparation and measurement approach, the authors refer to the experimental procedure described in Section 4.

As the porosities and layer thicknesses of the pristine and calendered electrode sheets represent key parameters for the evaluation of the thermal properties, these are given in **Table 1**. The uncertainties are determined according to the Guide to the Expression of Uncertainty in Measurement (GUM),[45] whereby the error margin of the measurement devices, especially the micrometer screw, have a far higher impact than the statistical deviation of the samples. The compression rate $\Pi_{c,i}$ is, herein, defined by Equation (2) following Haselrieder et al.,[30] whereby $s_{co,0}$ is the coating thickness of the pristine electrode and $s_{co,i}$ is the coating thickness of the calendered sheet $i$.
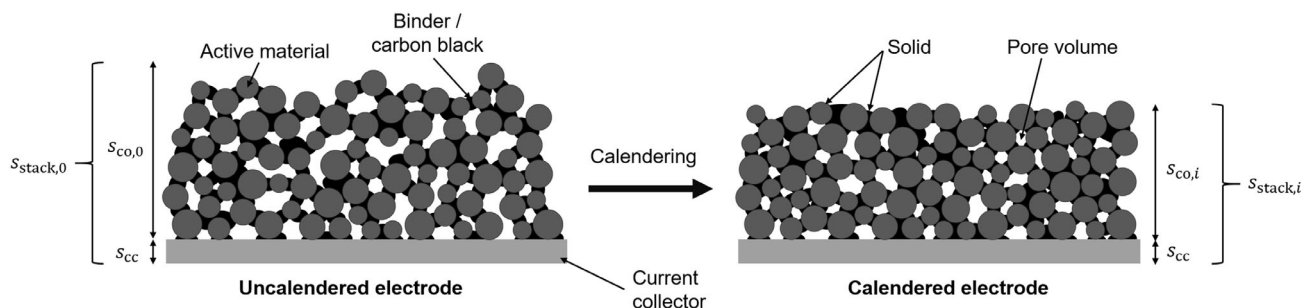


**Figure 1.** Schematic depiction of the thickness and porosity changes caused by the calendering process.

**2300259 (2 of 12)**

**ADVANCED
SCIENCE NEWS**

www.advancedsciencenews.com

**Energy Technology**
Generation, Conversion, Storage, Distribution

www.entechnol.de

**Table 1.** Mean values of the areal mass loading $m_a$, current collector thickness $s_{cc}$, porosity $\phi$, layer thickness of the coating $s_{co,i}$, and compression rate $\Pi_{c,i}$ of the uncalendered and calendered electrode sheets with the combined uncertainty according to GUM. The values are referred to as the thickness measurements with the micrometer screw using five samples per sheet and ten measurements per sample (see Section 4).

| | Sheet number | Porosity $\phi$ [–] | Layer thickness $s_{co,i}$ [µm] | Compression rate $\Pi_{c,i}$ [–] |
|---|---|---|---|---|
| Graphite$_{thin}$ | 1 | $0.606 \pm 0.063$ | $70.0 \pm 1.6$ | 0 |
| $m_a = 55.3\,\mathrm{g\,m^{-2}}$ | 2 | $0.586 \pm 0.071$ | $61.6 \pm 1.6$ | $0.121 \pm 0.019$ |
| $s_{cc} = 10.3 \pm 1.2\,\mathrm{µm}$ | 3 | $0.544 \pm 0.078$ | $55.8 \pm 1.6$ | $0.203 \pm 0.019$ |
| | 4 | $0.471 \pm 0.088$ | $48.5 \pm 1.6$ | $0.307 \pm 0.018$ |
| | 5 | $0.376 \pm 0.102$ | $40.8 \pm 1.6$ | $0.418 \pm 0.017$ |
| | 6 | $0.328 \pm 0.113$ | $37.0 \pm 1.8$ | $0.471 \pm 0.020$ |
| Graphite$_{thick}$ | 1 | $0.597 \pm 0.038$ | $117.2 \pm 1.7$ | 0 |
| $m_a = 98.2\,\mathrm{g\,m^{-2}}$ | 2 | $0.585 \pm 0.041$ | $108.2 \pm 1.7$ | $0.0766 \pm 0.0127$ |
| $s_{cc} = 11.0 \pm 1.2\,\mathrm{µm}$ | 3 | $0.569 \pm 0.043$ | $102.9 \pm 1.7$ | $0.122 \pm 0.012$ |
| | 4 | $0.514 \pm 0.049$ | $89.1 \pm 1.7$ | $0.240 \pm 0.012$ |
| | 5 | $0.412 \pm 0.049$ | $86.3 \pm 1.8$ | $0.264 \pm 0.013$ |
| | 6 | $0.291 \pm 0.058$ | $71.0 \pm 1.7$ | $0.394 \pm 0.011$ |
| | 7 | $0.211 \pm 0.068$ | $59.9 \pm 1.7$ | $0.489 \pm 0.011$ |
| NMC622 | 1 | $0.513 \pm 0.012$ | $54.9 \pm 1.6$ | 0 |
| $m_a = 114\,\mathrm{g\,m^{-2}}$ | 2 | $0.469 \pm 0.013$ | $50.4 \pm 1.6$ | $0.0813 \pm 0.0229$ |
| $s_{cc} = 16.7 \pm 1.2\,\mathrm{µm}$ | 3 | $0.427 \pm 0.015$ | $47.1 \pm 1.6$ | $0.141 \pm 0.022$ |
| | 4 | $0.379 \pm 0.018$ | $43.2 \pm 1.7$ | $0.213 \pm 0.021$ |
| | 5 | $0.349 \pm 0.019$ | $41.4 \pm 1.7$ | $0.245 \pm 0.021$ |
| | 6 | $0.303 \pm 0.021$ | $39.6 \pm 1.7$ | $0.279 \pm 0.021$ |
| NMC811 | 1 | $0.507 \pm 0.008$ | $79.5 \pm 1.6$ | 0 |
| $m_a = 172\,\mathrm{g\,m^{-2}}$ | 2 | $0.494 \pm 0.011$ | $75.5 \pm 1.6$ | $0.0499 \pm 0.0168$ |
| $s_{cc} = 16.2 \pm 1.2\,\mathrm{µm}$ | 3 | $0.488 \pm 0.008$ | $73.6 \pm 1.6$ | $0.0744 \pm 0.0166$ |
| | 4 | $0.483 \pm 0.009$ | $73.5 \pm 1.6$ | $0.0759 \pm 0.0166$ |
| | 5 | $0.472 \pm 0.009$ | $73.0 \pm 1.6$ | $0.0818 \pm 0.0166$ |
| | 6 | $0.454 \pm 0.010$ | $69.6 \pm 1.6$ | $0.125 \pm 0.016$ |
| | 7 | $0.372 \pm 0.012$ | $65.4 \pm 1.6$ | $0.178 \pm 0.016$ |
| | 8 | $0.319 \pm 0.015$ | $58.6 \pm 1.7$ | $0.263 \pm 0.016$ |

$$\Pi_{c,i} = \frac{s_{co,0} - s_{co,i}}{s_{co,0}} \quad (2)$$

Table 1 shows that far higher compression rates can be reached for the graphite anodes compared to the NMC cathodes. This can be explained by the higher starting porosity and lower compression resistance of the graphite anodes.[26]

Hereby, it is important that the porosity is not the only factor that is impacted by the compression during the calendering process. The microstructure of the coating can be altered in ways that are not yet completely understood. Additionally, the interface between the coating and the current collector is affected. Thus, it is more accurate to talk about the compression rate instead of porosity, when trying to include all impact factors of the calendering process. Nevertheless, the porosity was chosen for the depiction of the results in this study to allow a realistic comparison with existing models and to provide a simplified classification for the reader.

For enhanced understanding, the graphical representation with respect to the compression rate is given in the Supplementary Information.
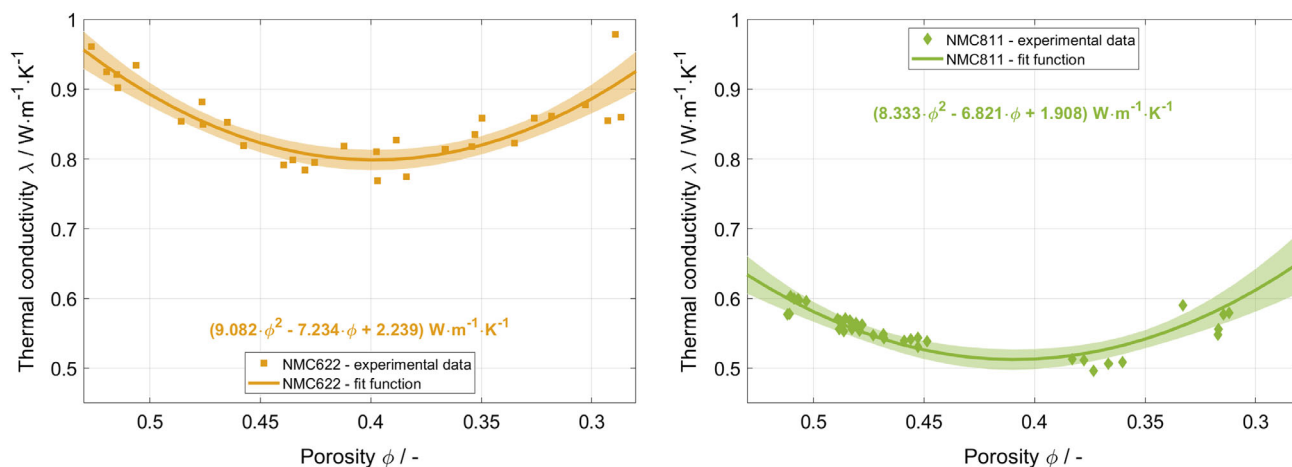
## 2.1. Effective Thermal Conductivity

With the measurement data for the effective thermal diffusivity $\kappa_{stack}$ of the calendered single-sided coated electrodes, the density $\rho$ and specific heat capacity $c_p$ of the solid materials and the porosity $\phi$ of the coating, the effective thermal conductivity $\lambda_{stack}$ of the electrode results from Equation (3).

$$\lambda_{stack} = \kappa_{stack}$$
$$\cdot \left[ \rho_{s,co} \cdot c_{p,s,co} \cdot (1 - \phi) \cdot \frac{s_{stack} - s_{cc}}{s_{stack}} + \rho_{cc} \cdot c_{p,cc} \cdot \frac{s_{cc}}{s_{stack}} \right] \quad (3)$$

The index "co" hereby describes the coating, "s" the solid material, "cc" the current collector, and "stack" the one-sided coated electrode consisting of both "co" and "cc". The thickness of the current collector $s_{cc}$ was assumed to not be significantly impacted by the compression during calendering following the observation of an elongation of the samples of less than one percent during the calendering process by Mayer et al.[36] Therefore, a constant value was used for the current collector thickness for all samples of one material. The heat capacity of the pore volume was neglected in this calculation. Further information on this can be found in Section 4 of this article, describing the experimental work. The results for the effective thermal conductivities of the cathode stacks as a function of the porosity are shown in **Figure 2**. Hereby, the single data points for the five samples per calendered sheet are given. The respective compression rates are given in Table 1. Under careful consideration of the measurement uncertainties of the devices, the results for both cathode types indicate a decrease in the thermal conductivity with a decreasing porosity until a minimum is reached at approx. $\phi = 0.4$ for both NMC622 and the NMC811. For a further decreasing porosity the thermal conductivity increases again.

A similar behavior was observed for the adhesion strength between the coating and the current collector of NMC cathodes in different studies. Hereby, the adhesion strength also first decreases and then increases again with decreasing porosity. This observation suggests that the alteration of the effective thermal conductivity during calendering might be significantly impacted by the connection at the interface between the coating and the current collector. The reduction of the adhesion strength is said to originate from sheer forces between the two layers during the calendering process, which impairs the connection.[37] When the line loads get high enough, the active material particles are pressed into the aluminum current collector foil and interlock with it leading to better contact and higher adhesion strength.[37] The penetration of active material particles into the current collector was observed by many authors for cathodes with rigid active material particles like NMC and LFP[27,28,36–40] and can also be seen for the most strongly calendered NMC622 cathode in this study in **Figure 3**. Here, the scanning electron microscopy (SEM) images of ion-milled cross-sections of three

ADVANCED
SCIENCE NEWS
www.advancedsciencenews.com

Energy Technology
Generation, Conversion, Storage, Distribution

www.entechnol.de

**Figure 2.** Effective thermal conductivity of the NMC622 (left) and NMC811 (right) cathode stacks. Data of the single samples in dependence on the porosity at a set temperature of 20 °C and quadratic fit functions with a 95% confidence interval. The measurement uncertainties of the different measurement devices are given in Section 4 of this article.

NMC622 cathodes with increasing compression rates are depicted. While the less strongly calendered samples do not show any penetration of the particles into the current collector, the particles are pressed into the current collector for the most strongly calendered sample. As a similar qualitative course of the adhesion strength was found for different cathode compositions with polyvinylidene fluoride (PVDF) binder, NMC111 or NMC622 active material, with and without graphite additive and different mass fractions of binder and carbon black,[27,28,37] it is assumed that the course is transferable to the cathodes in this work. An analysis of the adhesion strength of the hereby used electrodes could give an interesting insight. However, it lies without the scope of this work and could not be conducted due to the limited amount of sample material. The authors suggest an investigation of the direct connection of the adhesion strength and effective thermal conductivity in future work.

With the knowledge of this interface evolution during the calendering process, it can be assumed that the quality of the thermal contact also changes accordingly. Since the effective thermal conductivity measured in this study also includes the thermal contact resistance between the coating and current collector, the effective value is likely significantly impacted by this effect.

It needs to be noted that changes in the adhesion strength are only a measure of changes at the interface. Beyond that, there can also be changes in the structure of the coating itself. It is assumed that delamination or breakage of binder connections could occur for minor compression rates during the calendering process, but there is no literature describing this behavior known to the authors. A far more commonly observed behavior is the breaking of particles themselves,[24,46] which can happen for very high line loads. It was also found for the most strongly calendered cathode in this study (Figure 3) and can be also seen to some extent for sheet no. 4.

Considering the behavior of the thermal diffusivity in **Figure 4**, both the improvement of the thermal contact at the interface and the deterioration of the thermal transport path within the coating and thus its thermal diffusivity seem to

balance each other out for the NMC622 cathode leading to a plateau in the thermal diffusivity for lower porosities. Therefore, the results in Figure 4 suggest that the increase in the thermal conductivity for the lower porosities is only obtained by the increase of the volumetric heat capacity of the stack due to the reduction of the porosity. The thermal diffusivity and volumetric heat capacity for all the different electrode types are given in the Supplementary Information. The NMC811 cathode hereby shows a similar trend as described for the NMC622 material.

Only a few publications investigating the electrical conductivity with respect to the porosity are known. However, they provide interesting information for a comparison of the thermal and electrical behavior. Measurements by Sangrós Giménez et al.[46] suggest an increase of the electrical conductivity of NMC111 cathode stacks with decreasing porosity (from $\phi = 0.417$ to $\phi = 0.270$), which is the same range of porosity in which the thermal conductivity measured in this study is increasing. However, the sample with the highest porosity of $\phi = 0.417$ was already calendered. So, the publication does not give an insight into possible changes between the uncalendered sheet ($\phi = 0.522$) and the least strongly calendered sheet. Thus, it leaves unclear, if a decrease in the electrical conductivity appears in this range as it does for the effective thermal conductivity. A similar behavior with a monotonously increasing electrical conductivity with increased compression rate was found by Zhang et al.[47]

Additionally, it can be derived from Figure 2 that the effective thermal conductivity of the NMC622 stacks is between 25% and 60% higher than the effective thermal conductivity of the NMC811 stacks. However, regarding the data presented in this study, it cannot be concluded that the thermal conductivity of NMC622 (both active material particles and coated electrode stacks) is generally higher than the one of NMC811 as the electrodes have different compositions. The NMC622 cathode used in this study has both a higher carbon black mass fraction and additional graphite particles, which both have a significantly higher thermal conductivity than the active material with approx. $24\,\text{W}\,\text{m}^{-1}\,\text{K}^{-1}$ for carbon black[48] and a mean value of $130\,\text{W}\,\text{m}^{-1}\,\text{K}^{-1}$[43] to $139\,\text{W}\,\text{m}^{-1}\,\text{K}^{-1}$[49] for graphite.
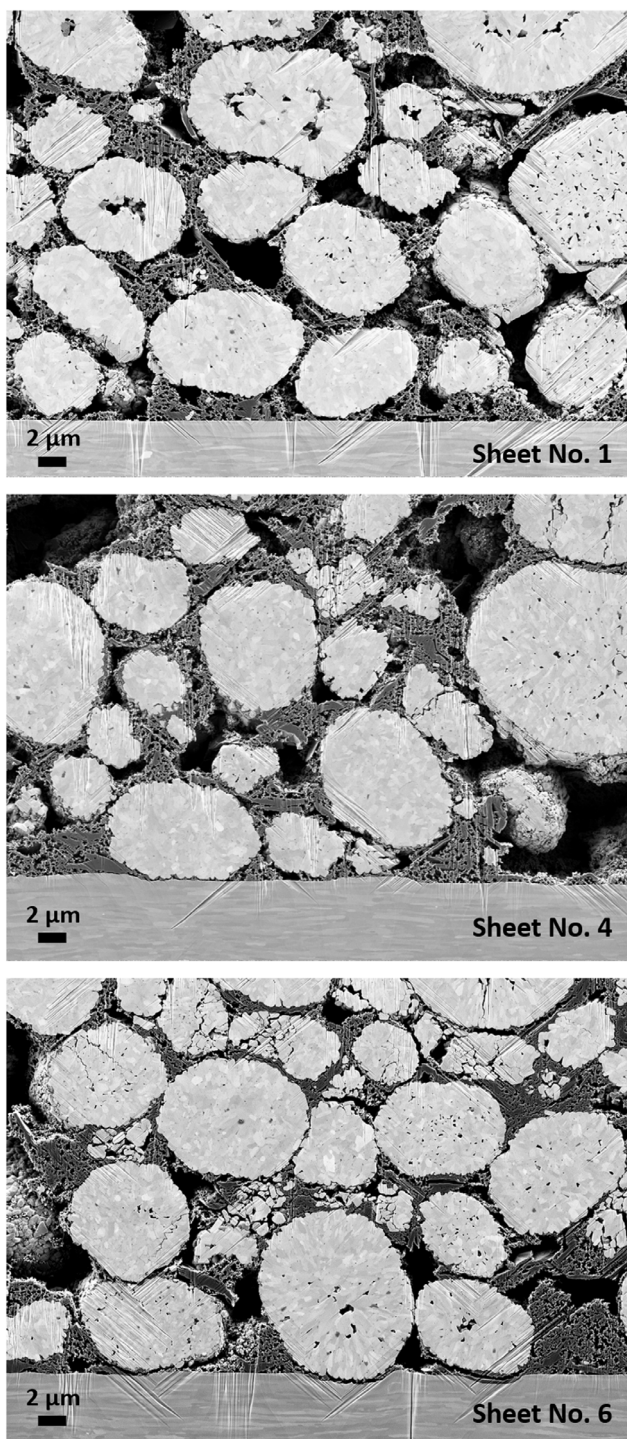
**Figure 3.** SEM images of ion-milled cross-sections of the NMC622 cathodes: Uncalendered sample (top), sheet at the minimum of the thermal conductivity (center), and most strongly calendered sample (bottom).

Furthermore, the coating of the NMC811 cathode is thicker, leading to a lower fraction of the highly conductive aluminum foil and therefore a lower effective thermal conductivity.

The effective thermal conductivity of the graphite anodes (see **Figure 5**) shows an even more pronounced decrease and
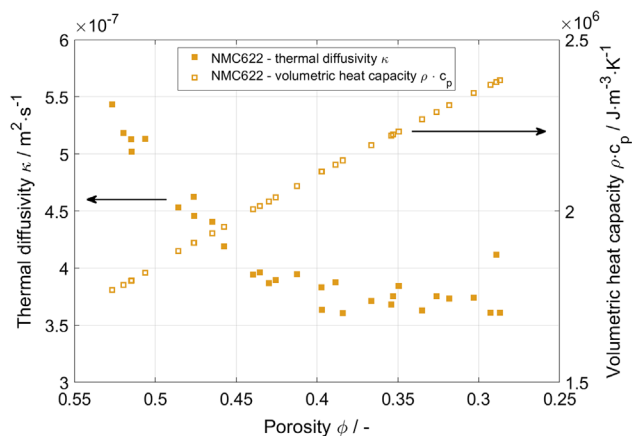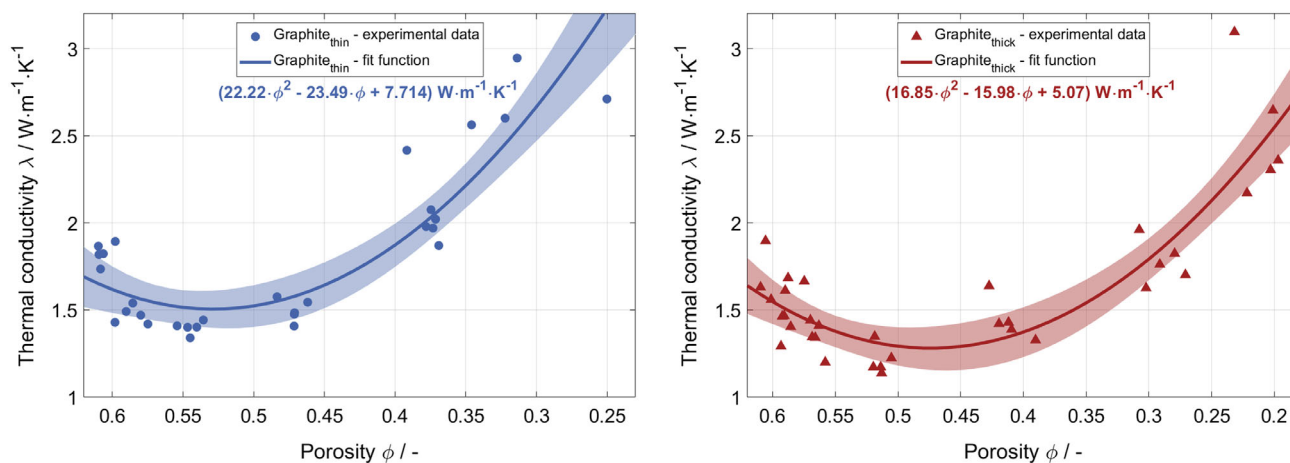


**Figure 4.** Effective thermal diffusivity of the NMC622 cathode stacks. Data of the single samples in dependence on the porosity at a set temperature of 20 °C.

then increase with decreasing porosity with a minimum at approx. $\phi = 0.54$ for the thin electrode and $\phi = 0.50$ for the thick electrode at a distinctly earlier stage of compression in comparison with the cathodes. Hereby, it is noteworthy that the values of the effective thermal conductivity of both electrode stacks are in the same order of magnitudes. Furthermore, both anodes show a strong scattering of the thermal conductivity and porosity for low porosities, which can be explained by the increased occurrence of defects due to the higher applied force.

There are two studies on the impact of the calendering process on the electrode properties of anodes known to the authors. The first study does not show a clear u-shape for the adhesion strength between graphite anode coatings and the copper current collector. Instead, a clearly increasing slope with decreasing porosity was found for high calender temperatures (125 °C) by Billot et al.[29] For lower temperatures, which are comparable to this work, the results by Billot et al.[29] do not show a clear tendency. However, PVDF was used as binder in this study, which might show a significantly different behavior than the carboxymethyl cellulose (CMC) styrene-butadiene rubber (SBR) combination. In the second study by Scheffler et al.,[50] using a CMC-SBR binder system with carbon additive similar to the one in this work, a u-shaped course was found for the adhesion strength between coating and current collector. This encourages the same assumptions that were made for the cathodes, suggesting that the effective thermal conductivity is impacted by the thermal contact resistance which is a measure of the quality of the interface between the coating and the current collector.

However, no deterioration and then improvement of the connection at the interface can be seen in the SEM images of the cross-section of differently strong calendered samples in **Figure 6**. The most strongly calendered sample even seems to show a slight gap between the coating and the current collector which can be explained by the strong shearing for high compression rates during calendering. This is said to be specifically strong for graphite electrodes and might entail a partial delamination of the coating. The thermal diffusivity shows the tendency to a u-shaped slope for both anodes in contrast to the cathodes (see Supporting Information), but leaves unclear if the increase

**Figure 5.** Effective thermal conductivity of the thin graphite (left) and thick graphite (right) anode stacks. Data of the single samples in dependence on the porosity at a set temperature of 20 °C and quadratic fit functions with a 95% confidence interval. The measurement uncertainties of the different measurement devices are given in the experimental section of this article.

originates from the better conduction within the coating or a reduction of the contact resistance.

Depicted here is the effective thermal conductivity of the electrode stack as a serial connection of the current collector and coating. As the current collector has approximately the same thickness for both electrodes, its fraction and thus the share of the better-conducting material is significantly lower for the thick graphite electrode. This leads to slightly higher values for the thin anode, although they could partially be attributed to the uncertainty of the measurements. Furthermore, higher coating thicknesses, described as higher area weights, showed lower adhesion strength in other studies for cathodes[27] and anodes.[29] Based on this knowledge, we assume that the thermal contact resistance might vary between the two electrodes as well and might also show a different course in dependence on the porosity.

Comparing the effective thermal conductivities of the anodes and cathodes, it is apparent that the anodes provide a far better heat conduction. This can not only be explained by the much higher thermal conductivity of graphite in comparison to NMC but also by the binder matrix. While the poorly conducting binder/carbon black phase takes up less than 6% of the solid volume fraction for the anode coatings, its volume fraction adds up to 11% (NMC811) to 13% (NMC622) for the cathode coatings. Furthermore, the cathodes show a high internal porosity of the binder matrix (see Supplementary Information), further reducing the thermal conductivity of the connecting phase. Additionally, the rather soft graphite particles allow plastic deformation resulting in larger contact areas between the particles and toward the interface, which also entails a higher effective thermal conductivity.

## 2.2. Uncertainty of the Layer Thickness

Measuring the accurate thickness of very thin samples is very challenging. It requires a high precision of the used measurement devices and has the risk of compressing the samples during the measuring process due to the applied pressure. Thus, it is beneficial to use different methods for the determination of the layer thickness to evaluate the uncertainty. Furthermore, an estimation of the impact of the uncertainty on the thermal conductivity is essential to quantitatively evaluate the resulting error.
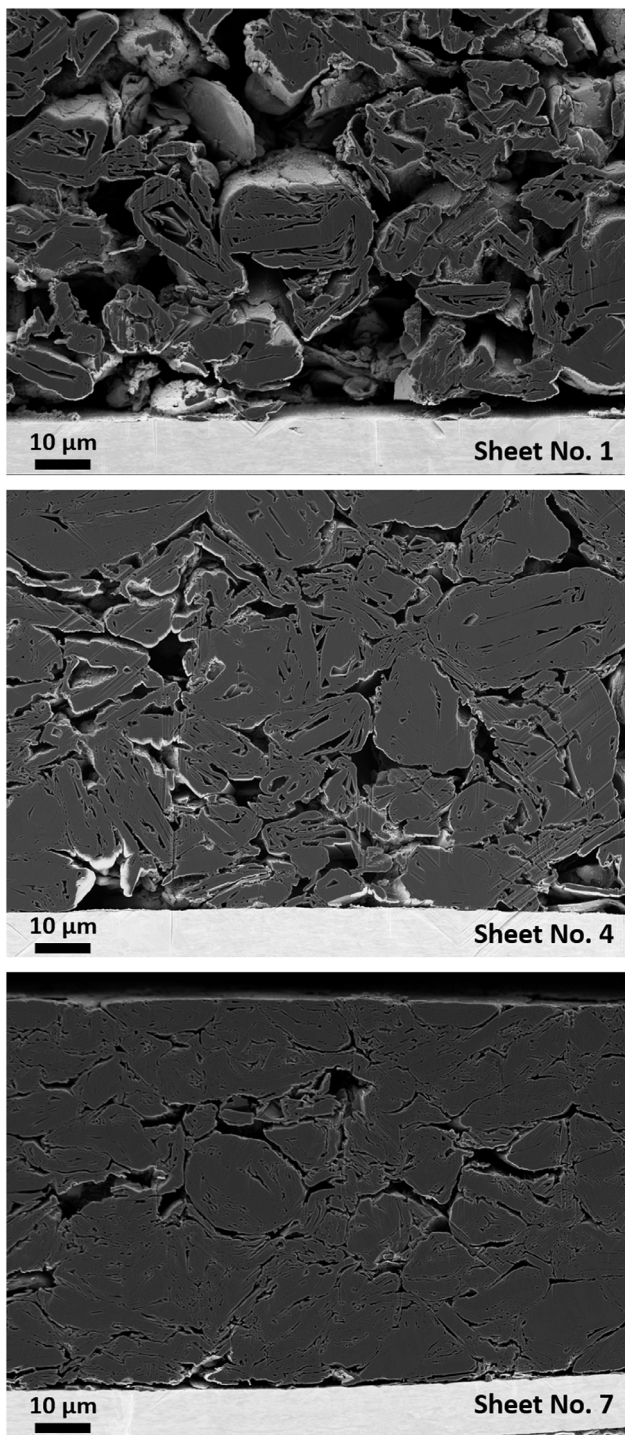
An error in the thickness affects different steps of the determination of thermal conductivity. First, it has an influence on the evaluation of the thermal diffusivity from the laser flash analysis (LFA) measurements according to Equation (4).[51]

$$\kappa = \frac{1.38 \, s^2}{\pi^2 t_{1/2}} \tag{4}$$

Besides the thickness $s$, the thermal diffusivity $\kappa$ is determined by the time $t_{1/2}$ passing until half of the measured temperature change is reached[51]. Thus, the higher the assumed thickness, the higher is the calculated thermal diffusivity, as the time is fixed by the measurement results and thus larger values of the transport properties are needed for the heat to be conducted along the same path inside the material at the same time. As the thermal conductivity is directly proportional to the thermal diffusivity, this also leads to higher values of the former.

Second, the thickness is an important part of the calculation of the porosity. For a known mass, solid density, and diameter of the sample, an increase in the thickness leads to a higher calculated porosity as the incorrectly higher assumed volume only leads to higher amounts of hollows (see Equation (6) in Section 4). The higher porosity itself leads to a lower effective thermal conductivity according to Equation (2).

And third, the thicknesses of stack and current collector also feed directly into the thermal conductivity through Equation (2). Hereby, only the relation of the two values is important and not the absolute values. For the investigation in this work, the ratio of $s_{cc}$ to $s_{stack}$ was assumed to stay constant, thus neglecting the interrelation of measurement uncertainties of the stack and current collector.

**ADVANCED
SCIENCE NEWS**

www.advancedsciencenews.com

**Energy Technology**
Generation, Conversion, Storage, Distribution

www.entechnol.de

**Figure 6.** SEM images of ion-milled cross-sections of the thick graphite anodes: Uncalendered sample (top), sheet at the minimum of the thermal conductivity (center), and most strongly calendered sample (bottom).
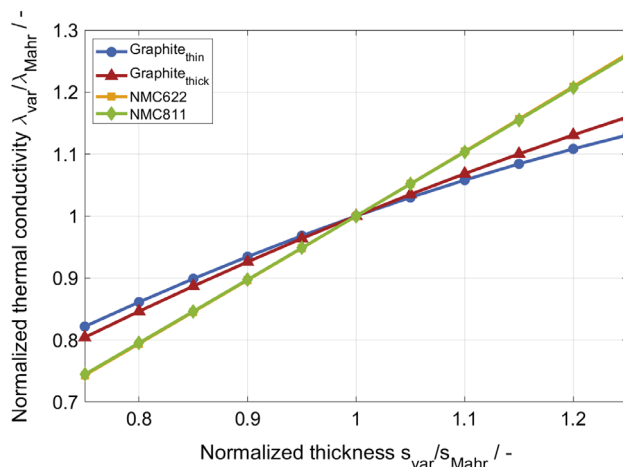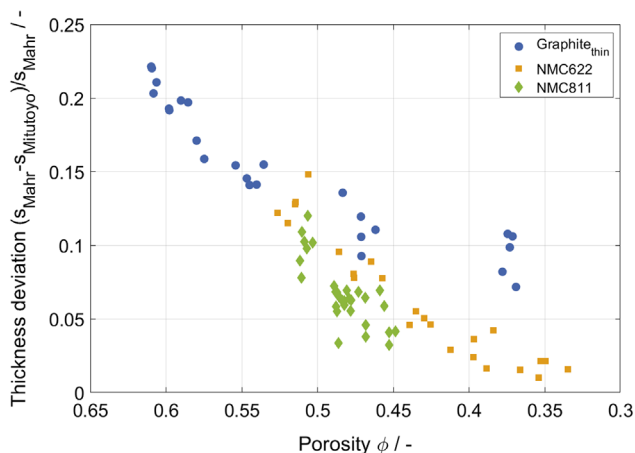


**Figure 7.** Impact of deviations in the measured electrode stack thickness on the effective thermal conductivity. Normalized to the absolute value for the thickness measured with the micrometer screw (Mahr GmbH).

for the varied thicknesses normalized to the thickness measured with the micrometer screw is depicted in **Figure 7**. Hereby, the thermal conductivity was also normalized to the value determined for the thickness from the micrometer screw measurements. Only the variation for the uncalendered samples is depicted here, but selected calendered samples led to similar results.

The effects of the thickness on thermal diffusivity and porosity are counteracting each other when it comes to the calculation of the thermal conductivity (see Equation (3)). The increasing slope of the effective thermal conductivity indicates that the thermal diffusivity has a stronger impact on this relation than the porosity. As a result, the thermal conductivity shows significantly lower relative variations than the thermal diffusivity, originating from the counteracting effect of the porosity (see Supplementary Information). A maximum relative variation of the thermal conductivity of 26% for NMC622 can be derived by assuming a 25% higher thickness than measured with the micrometer screw. However, NMC622 only showed a maximum of 15% thickness deviations between the two measurement methods resulting in variations of the thermal conductivity of less than 26%. While the tendency is similar, the effect is not equally strong for the different materials, which is attributed to the different porosity ranges. However, the graphs for NMC622 and NMC811 are almost equal, making the yellow curve for NMC622 barely identifiable.

As described in detail in Section 4 of this article, various measurement devices were used for the determination of the thickness of the electrodes. Hereby, the measurements with the dial indicator (Mitutoyo Corporation) led to up to 23% lower values than the micrometer screw (Mahr GmbH) for both current collectors and coated electrodes. The positive values in **Figure 8** indicate that the values measured with the micrometer screw (Mahr GmbH) are generally higher than those measured with the dial indicator (Mitutoyo Corporation). Furthermore, the results depicted in Figure 8 show a clear tendency toward lower relative deviations with decreasing porosity.

The micrometer screw has a flat measuring area of 33.18 mm$^2$ and a measuring force of 5 to 10 N[52] leading to a pressure of up

To assess the possible extent of the error of the thermal conductivity, the results of selected samples have been evaluated for a range of $\pm 25\%$ around the thickness measured with the micrometer screw (Mahr GmbH). The thermal conductivity

**Figure 8.** The relative deviation of the stack thickness was measured with the dial indicator by Mitutoyo Corporation in comparison to the micrometer screw by Mahr GmbH.

to 0.3014 N mm$^{-2}$. It presumably shows a marginal compression of the sample and thereby practically provides the thickness at the highest points of the sample without balancing unevenness. In contrast, the dial indicator has a ball tip contact element with a diameter of 3 mm and measuring forces of up to 2 N.[53] As the ball tip has a significantly lower contact area for a penetration depth in the μm-range, it might measure the thickness in hollows at the surface. Furthermore, the low area leads to a higher applied pressure, which might lead to a slight compression of the sample. For a penetration depth of up to 20 μm in the graphite samples and up to 10 μm in the NMC samples in comparison to the thickness measured with the micrometer screw, a pressure of at least 10.6 N mm$^{-2}$ for graphite and 21.2 N mm$^{-2}$ for NMC is applied.

The decrease in the deviation with decreasing porosity could be attributed to the fact that the more compressed layers first have smaller hollows and thus a more even surface and second have already experienced a stronger compression, so a further pressure application does not have such a big impact anymore. The strong unevenness of uncalendered electrodes and the leveling of the surface were also shown by Meyer et al.[26] This assumption also explains that the graphite anode still shows substantial deviations of approx. 10% for porosities below 0.4 while the deviations of the NMC cathodes are already below 5% here. As graphite electrodes have a smaller compaction resistance,[26] lower pressures are needed for the compression, leading to higher penetration depths.

These investigations leave open the question of which thickness measurement method should be used for future analyses. Hereby, it is crucial to consider the application for which the thickness is used. The LFA measurements were evaluated using the penetration model by McMasters et al.[51] in this study. This model is used for porous samples and takes into account the surface roughness of the sample and how the laser or light beam does not just hit the surface, but partially even penetrates further into the pores. As the penetration depth is fitted to the recorded temperature signal and thus corrected automatically by the Proteus LFA Analysis software (NETZSCH-

Gerätebau GmbH),[54] it is suggested to use the height of the highest point of the sample as thickness for the LFA evaluation and thus the values measured with the micrometer screw are preferred.

For the calculation of the porosity, a definite decision between the two measurement methods is not possible. If the dial gauge with the ball tip really just measures the lowest points of the coating surface and if it is assumed that the high points and low points balance each other out, a mean value of both thickness values would be a good estimation for the determination of the porosity in the main part of the coating. However, it is statistically improbable that the dial gauge only measures the low points of the samples, although we have only measured very few points that were as high as the micrometer values or even higher (max. of 12.5% for NMC622, approx. 0% for Graphite$_{thin}$ and NMC811). This leads us to the assumption that the low values mainly originate from the compression of the material and makes the measured thickness inapplicable for investigations in which the electrode is not further compressed. We therefore only used the values measured with the micrometer screw for the LFA and porosity evaluations in this study.

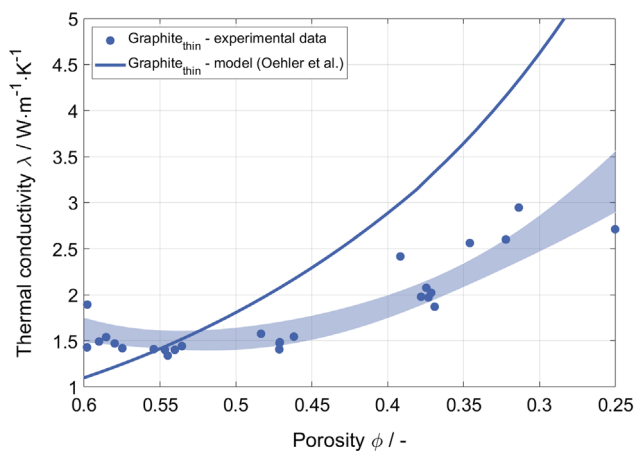### 2.3. Comparison with Model-Based Thermal Conductivities

It is known in the community that heat conduction models for simple packed beds cannot depict the complex relations of the microstructure within battery electrodes as they are influenced by many different effects. Thus, two models, which have been developed for the prediction of the thermal conductivity of porous electrode coatings, are compared to the newly measured data in this work.

The discrete element method (DEM) simulation model described by Sangrós et al.[43] is able to compare the impact of different particle sizes on the effective thermal conductivity, but neglects the binder/carbon black phase completely. Furthermore, the graphite particles are described by spheres although flat and uneven flake-like shapes are more realistic for this anode active material.[26]

The analytical model introduced by Oehler et al.[44] considers different heat conduction pathways through fluid, active material solid, and a combined phase. While the particle size is no contributing factor in this model, it is able to take into account particle shapes, different compositions as well as binder, and carbon black volume fractions.

**Figure 9** depicts the effective thermal conductivity of the thin graphite anode stack taken from the experiments and predicted with the model by Oehler et al.[44] assuming the same solid material composition and a continuum thermal conductivity of helium of 0.1518 W m$^{-1}$ K$^{-1}$ at 20 °C[55] within the pores. The mean values for the current collector and coating thickness were used for the calculation, containing more decimal places than the rounded values in Table 1. An anode was chosen as the graphite electrodes showed the best results for the validation of the model.[49] The model showed already significantly larger values for the cathodes than the experiments, according to Oehler.[49] This discrepancy between the values for the cathodes might be explained by the consideration of the binder phase. In

**ADVANCED
SCIENCE NEWS**

www.advancedsciencenews.com

**Energy Technology**
Generation, Conversion, Storage, Distribution

www.entechnol.de

**Figure 9.** Effective thermal conductivity of the thin graphite anode stacks. Experimentally determined data with 95% confidence interval and comparison with the calculated values according to the model by Oehler et al. in dependence on the porosity.

the model, the binder/carbon black is treated as a solid phase, whereas it can be seen from the SEM images in Figure 3 and a detailed depiction in the Supplementary Information that the binder matrix in our case has a significant porosity in itself, which might entail a considerable reduction of the thermal conductivity.

Furthermore, it should be mentioned that the thermal conductivity of the gas within the discontinuum of the small pores might be significantly smaller than the used continuum value due to the so-called Knudsen or Smoluchowski effect.[56,57] While this effect influences the absolute values of the effective thermal conductivity it does not seem to affect the qualitative course of the thermal conductivity within the given porosity range.

The utilized material properties of the single components and the results for the other electrodes can be found in the Supplementary Information. Hereby, only a porosity range of $\phi = 0.25$ to $\phi = 0.6$ was plotted as the model was only used in this region by Oehler.[49] To make the model comparable to the experimental results, the conduction through the current collector was taken into account using Equation (5), where $s_{stack}$, $s_{co,}$ and $\overline{\lambda}_{co}$ are functions of the porosity. The contact resistance between the coating and current collector hereby is comprised of the combined thermal conductivity of the coating $\overline{\lambda}_{co}$ as it was done for the validation of the model as well.[44]

$$\lambda_{stack} = \frac{s_{stack}}{\frac{s_{cc}}{\lambda_{cc}} + \underbrace{\frac{s_{co}}{\lambda_{co}} + R_{contact}}_{\frac{s_{co}}{\lambda_{co}}}} \tag{5}$$

While the experimental results for the thermal conductivity show a u-shaped slope, the results of the model indicate that the thermal conductivity steadily increases with decreasing porosity leading to much higher values than observed in the measurements. It has to be mentioned that the depicted results for the thin graphite electrode show the best fit of all investigated materials.

The results of the model by Sangrós et al.[43] show a similar behavior as the model by Oehler et al.[44] with a steady increase for the graphite anode material. Thus, both models are capable of roughly describing the increasing slope for low porosities. However, they do not show a decreasing slope for low compression rates as it was found for the experimental data. Both models are based on the porosity as the main influencing factor, hence, they do not consider changes in the microstructure such as breakage or build-up of new connections, which probably occur during the process of calendering.[37] Since the active material particles have a significantly higher thermal conductivity than the fluid phase, it is standing to reason that the effective thermal conductivity must increase with decreasing porosity and thus increasing volume fraction of the active material. Due to the assumptions made for both models with respect to the changes in the microstructure, they are not expected to be capable of describing the variation of the effective thermal conductivity during the calendering process accurately.

An important factor hereby might also be the way of considering the thermal contact resistance. Oehler[49] validated his model with experimental data from electrode stacks. Until now there is no option to measure the thermal conductivity of the coating separately, thus his measurements also contain the thermal contact resistance. However, by the evaluation of the measurements according to Oehler[49] using the combined value $\overline{\lambda}_{co}$ this resistance is included in the thermal conductivity of the coating. Therefore, the plotted results in Figure 9 both depict the combination of the conduction through coating and current collector and the thermal contact resistance and are thus comparable.

However, the model by Oehler[49] does not consider changes in this resistance as electrodes from commercial cells were used for the validation. The single electrodes had fixed porosities in the range of 28%–37% and varied material compositions making an adequate comparison very difficult. It should be noted that those electrodes have undergone a formation and cyclization. It is assumed that the process of formation might lead to a reduction of the contact resistance by the build-up of interfacial layers and thus entail a higher effective thermal conductivity explaining the slope in the model results. In contrast, our cells have not experienced a formation and not even been in contact with electrolytes.

As a result, it is assumed that the models were never meant to replicate the calendering process, but have rather been developed to describe the behavior of finalized battery electrodes within the lower porosity range.

This approach of the measurement evaluation with the inclusion of the contact resistance into the thermal conductivity of the coating does not influence the perpendicular thermal conductivity of the whole battery stack. However, it does lead to an underestimation of the thermal conductivity parallel to the layers. Thus, the distinction between thermal conductivity of the coating and the thermal contact resistance $R_{contact}$ according to the upper part of Equation (5) provides an approach closer to reality. This way the value can also be used for the more realistic calculation of the thermal conductivity parallel to the layers.

The same approach should be used for the perpendicular conduction through the whole battery stack to take into account the contact resistances between all the layers (anode, separator, and

**ADVANCED**
**SCIENCE NEWS**
www.advancedsciencenews.com

**Energy Technology**
Generation, Conversion, Storage, Distribution
www.entechnol.de

cathode). However, the determination of all contact resistances still brings challenges requiring further research in this field.

## 3. Conclusion

We investigated the dependence of the effective thermal conductivity of different electrode stacks on the compression rate for a specific calendering process, quantitatively described by the porosity. For all four of our electrode types, we could show a similar and significant dependence on the compression rate. A minimum in the effective thermal conductivity is reached for porosities of approx. $\phi = 0.4$ for cathodes and $\phi = 0.5$ to $\phi = 0.55$ for anodes.

The effective thermal conductivity seems to correlate with the adhesion strength between the coating and the current collector as a function of the porosity, encouraging the assumption that the effective value is significantly influenced by the behavior at the interface. This follows the hypothesis that a better mechanical contact comes along with an enhanced thermal contact. The increase in the effective thermal conductivity of the anodes for low porosities can be attributed to this effect as well.

These investigations lead us to the assumption that there is a thermal contact resistance between the coating and the current collector that significantly contributes to the overall thermal conduction through the electrode stack.

Moreover, we looked into the impact of uncertainties in the thickness measurements on the calculated thermal conductivity. The thickness value hereby feeds into the evaluation of the thermal diffusivity measurements and the calculation of the porosity, which have counteracting effects on thermal conductivity. The influence through the thermal diffusivity is stronger according to our results. The impact of an error in the relation between coating thickness and stack thickness was neglected in this study.

Our results also show a clear tendency toward smaller differences between the two thickness measurement methods for stronger calendered electrodes. This observation is attributed to an increasing resistance toward compression by the measurement device with increasing compression rate by calendering.

We showed that the neglection of the contact resistance does not change anything in the calculation of the perpendicular thermal conductivity of the whole battery stack, but it decreases the thermal conductivity parallel to the layers. Thus, we recommend a further investigation of the thermal contact resistances between the coating and the current collector as well as between the stacked layers, namely the electrodes and separator sheets.

Furthermore, the comparison of the experimental results with two modeling approaches from the literature showed a poor agreement of the data. This is most likely due to the fact, that the models do not take into account the changes that are caused within the microstructure by the calendering process, but only account for the change in porosity.

## 4. Experimental Section

For the sample preparation at the Institute of Applied Materials – Energy Storage Systems (IAM-ESS) single-side coated, uncalendered electrode sheets from the same batch were used. Before the calendering, they have been stored either in ambient air (graphite), in a desiccator with air

**Table 2.** Mass fractions in the coating in wt% and material of the current collector for both graphite anodes (same composition and current collector) and NMC622 and NMC811 cathodes.

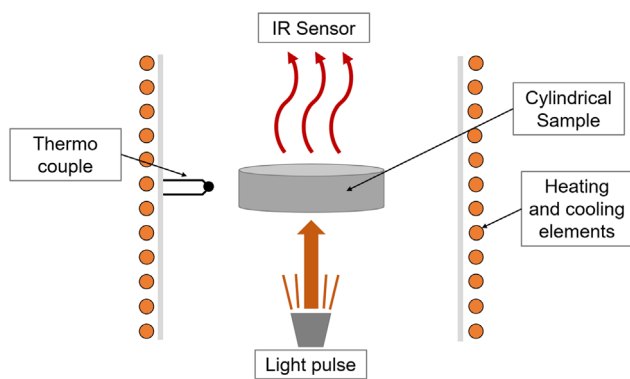| | Graphite$_{thin}$ Graphite$_{thick}$ | NMC622 | NMC811 |
|---|---|---|---|
| Active material | 96 | 92 | 96 |
| PVDF binder | – | 3.0 | 2.0 |
| CMC binder | 1.25 | – | – |
| SBR binder | 1.25 | – | – |
| Graphite additive | – | 2.0 | – |
| Conductive carbon black | 1.50 | 3.0 | 2.0 |
| Current collector | Copper | Aluminum | Aluminum |

(NMC622) or in inert atmosphere (NMC811), depending on their tendency to deteriorate during contact with oxygen and water. The solid material composition of the different electrodes in wt% is given in **Table 2**.

Four different coating batches of three different materials were calendered in air with different forces to reach samples with various layer thicknesses and different porosities. Hereby, a two-roll laboratory calender (GKL 200, Saueressig) with a roll diameter of 267 mm, width of 400 mm, and a circumferential velocity of 1 m min$^{-1}$ was used. The temperature was set to a constant value of 50 °C. Directly after the calendering process, the layer thicknesses were measured with a dial gauge for a first indication of the compression rate. After the calendering, the samples were dried in air at a temperature of 50 to 60 °C overnight and then stored within a dry glovebox with inert argon atmosphere. To keep the air contact as low as possible the sample preparation was mainly conducted within the glovebox so that the samples were only exposed to air right before the measurement. This way it can be assumed that the impact on the mechanical and chemical structure and thereby also the thermal material properties can be neglected in this work. All measurements of density, specific heat capacity, and thermal diffusivity were conducted at the Institute of Thermal Process Engineering (TVT). The specific heat capacities and densities were determined by differential scanning calorimetry (DSC) and gas pycnometry, respectively. Both properties were only measured for the solid particle mixture of the coatings as the values of the porous structure can then be calculated with the knowledge of the porosity. As the sheets are taken from the same batch with a consistent material composition and as it can be assumed that $\rho$ and $c_p$ do not change for the solid material during the calendering process, those measurements were not conducted for every single porosity. Instead, only the uncalendered electrode sheets were used for those investigations.

For the DSC measurements, the coating was scraped off the current collector and compactly pressed into standard aluminum crucibles. Three samples were prepared for each material. The measurements were conducted with a Q2000 (TA Instruments) with a measurement uncertainty of $\pm 0.05\%$ in nitrogen atmosphere with a flow rate of 50 mL min$^{-1}$. Hereby, a temperature range of $-40$ to 60 °C was run in 2 K steps with a heating rate of 20 K min$^{-1}$. The temperature ramp was performed five times for each sample.

The density measurements were conducted with an Ultrapyc 1200e (Quantachrome) with a measurement uncertainty of $\pm 0.03\%$, which allows the determination of the solid density of powders. Nitrogen was used as measuring gas at a set temperature of 25 °C. Three samples out of the scraped off solid material were gauged for each electrode composition.

The thermal diffusivity had been determined using laser flash analysis (LFA) measurements. The operating principle of the LFA is schematically depicted in **Figure 10**. Hereby, a light pulse is shot onto a tempered cylindrical sample and the temperature change on the opposite side is detected by an infrared sensor over time. For the sample preparation, coins were punched out of the electrode sheets. The thermal diffusivity was measured

ADVANCED
SCIENCE NEWS
www.advancedsciencenews.com

Energy Technology
Generation, Conversion, Storage, Distribution
www.entechnol.de

**Figure 10.** Schematic depiction of the laser flash method.

for every single porosity of each material. Hereby, five samples were prepared per sheet. To prevent reflection and increase the absorption of the light beam, the metal side of the samples was spray coated with a thin graphite layer (Äronix). As measurement device an LFA 467 Hyperflash (NETZSCH-Gerätebau GmbH) with a measurement uncertainty of $\pm 3\%$ was used with nitrogen as protective gas with a volume flow rate of 60 mL min$^{-1}$. All shown results were obtained in a helium atmosphere with a volume flow rate of 25 mL min$^{-1}$. A temperature range of $-20$ to 60 °C was investigated with measurements in 10 K intervals. The cooling below room temperature was achieved with liquid nitrogen. No further pressure was applied to the samples during the measurements. The light flash was shot onto the side with the electrode coating for all samples.

The evaluation of the LFA measurements was conducted with the Proteus LFA Analysis software (NETZSCH-Gerätebau GmbH). Due to the roughness of the porous samples the penetration model was used, which is comprehensively described by McMasters et al.[51]

The porosity was determined by gravimetrical measurements of the round electrode coins, which were prepared for the LFA measurements. With the knowledge of the densities of the current collector and the solid material of the coating and the mass and geometrical dimensions of the sample, the porosity may be calculated by Equation (6).

$$\phi = 1 - \left[ \frac{m_{\text{stack}}}{\left( \frac{\pi \cdot d^2}{4} \cdot s_{\text{co}} \right)} - \rho_{\text{cc}} \cdot \frac{s_{\text{cc}}}{s_{\text{co}}} \right] \cdot \rho_{\text{s,co}}^{-1} \tag{6}$$

In this study, the mass was measured with a Balance XPE206DR precision scale (Mettler Toledo) with a measurement uncertainty of $\pm 0.015$ mg and the diameter was measured with a digiMax 150D digital caliper (Wiha Werkzeuge GmbH) with a measurement uncertainty of $\pm 0.05$ mm. The punching out of the samples might lead to material loss on the edges, resulting in slightly reduced masses and higher porosities.

The thicknesses used for the evaluation of the results were measured with a digital micrometer screw Micromar 40 EWR (Mahr GmbH) with an error margin of 2 μm for all electrode samples and current collectors. Each of the five samples per sheet was measured 10 times. The results showed significant differences in comparison to the measurements taken with a dial gauge directly after the calendering process. To evaluate possible errors in the values used for the evaluation of the thermal conductivity approx. half of the samples were then again measured with a digital dial indicator ID-H0530 (Mitutoyo Corporation) with an accuracy of $\pm 1.5$ μm 10 times per sample.

As helium was used as fluid within the pores for the LFA measurements, the gaseous phase has been neglected in the evaluation, according to Equation (3). Investigations have shown that this simplification is valid, as the volumetric heat capacity $\rho_{\text{He}} \cdot c_{\text{p,He}}$ of helium is equivalent to only 0.024% (for NMC811) to 0.055% (for graphite) of the heat capacity of the solid mixture of the coating. Hereby, specific heat capacities of 701.1 J kg$^{-1}$ K$^{-1}$ (graphite), 785.8 J kg$^{-1}$ K$^{-1}$ (NMC622), and 773.5 J kg$^{-1}$ K$^{-1}$ (NMC811) measured at 20 °C and densities of

2162 kg m$^{-3}$ (graphite), 4229 kg m$^{-3}$ (NMC622), and 4474 kg m$^{-3}$ (NMC811) measured at approx. 24 °C for the solid mixtures were used for the calculation.

## Supporting Information

Supporting Information is available from the Wiley Online Library or from the author.

## Conflict of Interest

The authors declare no conflict of interest.

## Data Availability Statement

The data that support the findings of this study are available from the corresponding author upon reasonable request.

[1] M. Fleckenstein, O. Bohlen, M. A. Roscher, B. Bäcker, *J. Power Sources* **2011**, *196*, 4769.

[2] Y. Troxler, B. Wu, M. Marinescu, V. Yufit, Y. Patel, A. J. Marquis, N. P. Brandon, G. J. Offer, *J. Power Sources* **2014**, *247*, 1018.

[3] D. Werner, S. Paarmann, A. Wiebelt, T. Wetzel, *Batteries* **2020**, *6*, 13.

[4] D. Werner, S. Paarmann, A. Wiebelt, T. Wetzel, *Batteries* **2020**, *6*, 12.

[5] S. Paarmann, L. Cloos, J. Technau, T. Wetzel, *Energy Technol.* **2021**, *158*, 2000862.

[6] G. Offer, Y. Patel, A. Hales, L. Bravo Diaz, M. Marzook, *Nature* **2020**, *582*, 485.

[7] I. A. Hunt, Y. Zhao, Y. Patel, G. J. Offer, *J. Electrochem. Soc.* **2016**, *163*, A1846.

[8] H. Maleki, S. A. Hallaj, J. R. Selman, R. B. Dinwiddie, H. Wang, *J. Electrochem. Soc.* **1999**, *146*, 947.

[9] D. Werner, A. Loges, D. J. Becker, T. Wetzel, *J. Power Sources* **2017**, *364*, 72.

[10] P. Gotcu, W. Pfleging, P. Smyrek, H. J. Seifert, *Phys. Chem. Chem. Phys.* **2017**, *19*, 11920.

[11] F. Richter, S. Kjelstrup, P. J. S. Vie, O. S. Burheim, *J. Power Sources* **2017**, *359*, 592.

[12] M. Koller, J. Unterkofler, G. Glanz, D. Lager, A. Bergmann, H. Popp, *Batteries* **2022**, *8*, 16.

**ADVANCED
SCIENCE NEWS**

www.advancedsciencenews.com

**Energy Technology**
Generation, Conversion, Storage, Distribution

www.entechnol.de

[13] M. Steinhardt, J. V. Barreras, H. Ruan, B. Wu, G. J. Offer, A. Jossen, *J. Power Sources* **2022**, *522*, 230829.

[14] Z. Li, J. Zhang, B. Wu, J. Huang, Z. Nie, Y. Sun, F. An, N. Wu, *J. Power Sources* **2013**, *241*, 536.

[15] J. Fleming, T. Amietszajew, J. Charmet, A. J. Roberts, D. Greenwood, R. Bhagat, *J. Energy Storage* **2019**, *22*, 36.

[16] S. C. Chen, C. C. Wang, Y. Y. Wang, *J. Power Sources* **2005**, *140*, 111.

[17] X. Cui, J. Zeng, H. Zhang, J. Yang, J. Qiao, J. Li, W. Li, *Int. J. Energy Res.* **2020**, *44*, 3640.

[18] O. Queisser, L. Cloos, F. Boehm, D. Oehler, T. Wetzel, *Energy Technol.* **2021**, *6*, 2000915.

[19] W. Haselrieder, B. Westphal, H. Bockholt, A. Diener, S. Höft, A. Kwade, *Int. J. Adhes.* **2015**, *60*, 1.

[20] W. Bauer, D. Nötzel, V. Wenzel, H. Nirschl, *J. Power Sources* **2015**, *288*, 359.

[21] H. Bockholt, W. Haselrieder, A. Kwade, *Powder Technol.* **2016**, *297*, 266.

[22] B. Westphal, H. Bockholt, T. Günther, W. Haselrieder, A. Kwade, *ECS Trans.* **2015**, *64*, 57.

[23] J. Klemens, L. Schneider, E. C. Herbst, N. Bohn, M. Müller, W. Bauer, P. Scharfer, W. Schabel, *Energy Technol.* **2022**, *10*, 2100985.

[24] H. Bockholt, *Formulierungstechniken Für Eigenschaftsoptimierte Lithiumionenbatterieelektroden*, Sierke Verlag, Göttingen, Germany, **2016**.

[25] H. Bockholt, M. Indrikova, A. Netz, F. Golks, A. Kwade, *J. Power Sources* **2016**, *325*, 140.

[26] C. Meyer, H. Bockholt, W. Haselrieder, A. Kwade, *J. Mater. Process. Technol.* **2017**, *249*, 172.

[27] C. Meyer, M. Weyhe, W. Haselrieder, A. Kwade, *Energy Technol.* **2020**, *8*, 1900175.

[28] D. Schreiner, M. Oguntke, T. Günther, G. Reinhart, *Energy Technol.* **2019**, *7*, 1900840.

[29] N. Billot, T. Günther, D. Schreiner, R. Stahl, J. Kranner, M. Beyer, G. Reinhart, *Energy Technol.* **2020**, *8*, 1801136.

[30] W. Haselrieder, S. Ivanov, D. K. Christen, H. Bockholt, A. Kwade, *ECS Trans.* **2013**, *50*, 59.

[31] C. Fongy, A.-C. Gaillot, S. Jouanneau, D. Guyomard, B. Lestriez, *J. Electrochem. Soc.* **2010**, *157*, A885.

[32] C.-W. Wang, Y.-B. Yi, A. M. Sastry, J. Shim, K. A. Striebel, *J. Electrochem. Soc.* **2004**, *151*, A1489.

[33] C. Schilcher, C. Meyer, A. Kwade, *Energy Technol.* **2016**, *4*, 1604.

[34] B. Bold, J. Fleischer, *ZWF Z. wirtschaftlich. Fab.* **2018**, *113*, 571.

[35] T. Günther, D. Schreiner, A. Metkar, C. Meyer, A. Kwade, G. Reinhart, *Energy Technol.* **2020**, *8*, 1900026.

[36] D. Mayer, A.-K. Wurba, B. Bold, J. Bernecker, A. Smith, J. Fleischer, *Processes* **2021**, *9*, 2009.

[37] W. Haselrieder, *Kalandrierung Zur Gezielten Einstellung Der Batterieelektroden-Performance*, Sierke Verlag, Göttingen, Germany, **2017**.

[38] H. Y. Tran, G. Greco, C. Täubert, M. Wohlfahrt-Mehrens, W. Haselrieder, A. Kwade, *J. Power Sources* **2012**, *210*, 276.

[39] A. van Bommel, R. Divigalpitiya, *J. Electrochem. Soc.* **2012**, *159*, A1791.

[40] D. Schmidt, M. Kamlah, V. Knoblauch, *J. Energy Storage* **2018**, *17*, 213.

[41] P. Novák, W. Scheifele, O. Haas, *J. Electrochem. Soc.* **1997**, *68*, 267.

[42] H. Maleki, J. R. Selman, R. B. Dinwiddie, H. Wang, *J. Electrochem. Soc.* **2001**, *94*, 26.

[43] C. Sangrós, C. Schilde, A. Kwade, *Energy Technol.* **2016**, *4*, 1611.

[44] D. Oehler, P. Seegert, T. Wetzel, *Energy Technol.* **2021**, *9*, 2000574.

[45] Joint Committee for Guides in Metreology, Evaluation of measurement data – Guide to the expression of uncertainty in measurement, JCGM 100, September 2008, Geneva, Switz.

[46] C. Sangrós Giménez, C. Schilde, L. Froböse, S. Ivanov, A. Kwade, *Energy Technol.* **2020**, *8*, 1900180.

[47] J. Zhang, H. Huang, J. Sun, *Powder Technol.* **2022**, *409*, 117828.

[48] D. Oehler, J. Bender, P. Seegert, T. Wetzel, *Energy Technol.* **2020**, *9*, 2000722.

[49] D. Oehler, *Bestimmung Der Thermischen Transporteigenschaften Poröser Elektroden Von Lithium-Ionen Batterien*, Karlsruhe Institute of Technology (KIT), Karlsruhe, Germany, **2021**.

[50] S. Scheffler, R. Jagau, N. Müller, A. Diener, A. Kwade, *Batteries* **2022**, *8*, 46.

[51] R. L. McMasters, J. V. Beck, R. B. Dinwiddie, H. Wang, *J. Heat Transfer* **1999**, *121*, 15.

[52] Mahr GmbH, Integrated Wireless Familien – MarCal, Micromar, MarCator, **2020**, https://metrology.mahr.com/en-int/products/article/4157100-digitale-buegelmessschraube-micromar-40-ewri (accessed: January 2023).

[53] Mitutoyo Corporation, ID-H0530/0560 Digimatic Indicator – User's Manual No. 99MAH016B6 SERIES No. 543, https://shop.mitutoyo.de/web/mitutoyo/en_DE/mitutoyo/01.04.04A/Digital%20Indicator%20ID-H%2C%2°CEE%20AC-Adapter/$catalogue/mitutoyoData/PR/543-561D/index.xhtml (accessed: January 2023).

[54] NETZSCH-Gerätebau GmbH, Documentation Proteus LFA Analysis – Penetration Model.

[55] M. Kleiber, R. Joh, R. Span, in *VDI Heat Atlas* (Ed.: VDI e. V.), Springer Berlin, Heidelberg, Berlin, Germany **2010**, pp. 301–418.

[56] E.-U. Schlünder, E. Tsotsas, *Wärmeübertragung in Festbetten, durchmischten Schüttgütern und Wirbelschichten*, Thieme, Stuttgart, Germany, **1988**.

[57] S. Sonnick, L. Erlbeck, M. Meier, H. Nirschl, M. Rädle, *Int. J. Heat Mass Transfer* **2022**, *187*, 122519.

**2300259 (12 of 12)**